Divergent microtubule assembly rates after short- versus long-term loss of end-modulating kinesins

Linda Wordeman*, Justin Decarreau, Juan Jesus Vicente, and Michael Wagenbach
Department of Physiology and Biophysics, University of Washington School of Medicine, Seattle, WA 98195

ABSTRACT **Depletion of microtubule (MT) regulators can initiate stable alterations in MT assembly rates that affect chromosome instability and mitotic spindle function, but the manner by which cellular MT assembly rates can stably increase or decrease is not understood. To investigate this phenomenon, we measured the response of microtubule assembly to both rapid and long-term loss of MT regulators MCAK/Kif2C and Kif18A. Depletion of MCAK/Kif2C by siRNA stably decreases MT assembly rates in mitotic spindles, whereas depletion of Kif18A stably increases rates of assembly. Surprisingly, this is not phenocopied by rapid rapamycin-dependent relocalization of MCAK/Kif2C and Kif18A to the plasma membrane. Instead, this treatment yields opposite affects on MT assembly. Rapidly increased MT assembly rates are balanced by a decrease in nucleated microtubules, whereas nucleation appears to be maximal and limiting for decreased MT assembly rates and also for long-term treatments. We measured amplified tubulin synthesis during long-term depletion of MT regulators and hypothesize that this is the basis for different phenotypes arising from long-term versus rapid depletion of MT regulators.**

Monitoring Editor
Manuel Théry
CEA, Hopital Saint Louis

Received: Nov 24, 2015
Revised: Feb 8, 2016
Accepted: Feb 16, 2016

INTRODUCTION

A modest increase in microtubule (MT) polymerization rates is of serious consequence to the cell because increased MT assembly rates are directly correlated with a rise in chromosome instability (Ertych *et al.*, 2014). It is unknown how cellular MT assembly rates become stably increased in cells; previous studies showed that MT polymer/dimer partitioning is controlled to maintain a remarkably consistent MT polymer mass throughout the cell cycle (Zhai and Borisy, 1994). Here we investigate this phenomenon using two kinesin-related proteins, Kif18A and Kif2C/mitotic centromere–associated kinesin (MCAK), which are known to regulate MT end dynamics and whose MT end–modulating activities have been well characterized in vitro. This study was inspired by our previous observation that depletion of the kinesin Kif4A, which has been shown by many groups to suppress MT end dynamics (Bringmann *et al.*, 2004; Hu *et al.*, 2011; Stumpff *et al.*, 2012; Nunes Bastos *et al.*, 2013), leads to a modest increase in MT assembly rates that facilitates metaphase congression (Stumpff *et al.*, 2012; Wandke *et al.*, 2012) and spindle elongation (Hu *et al.*, 2011; Nunes Bastos *et al.*, 2013). These data suggest that modest increases in MT assembly rates might adversely affect mitotic spindle mechanisms. Although numerous genetic lesions manifest increased MT assembly rates (Stolz *et al.*, 2015), two kinesins, MCAK/Kif2C and Kif18A, are already well established as regulators assembly and disassembly of tubulin at MT ends (reviewed in Walczak *et al.*, 2013). MCAK/Kif2C is capable of catalytically depolymerizing MTs from either end (Hunter *et al.*, 2003; Cooper *et al.*, 2010), whereas Kif18A appears to suppress MT assembly and disassembly when a sufficient quantity translocates to MT plus ends (Du *et al.*, 2010; Stumpff *et al.*, 2011, 2012). Because these two kinesins have well-established but mechanistically distinct roles as MT assembly modulators, we investigated the influence of these two kinesins on MT assembly rates in live cells.

MCAK/Kif2C is a potent depolymerizer of MTs, yet it is enriched on the plus ends of polymerizing MTs via an interaction with end-binding protein 1 (EB1; Moore *et al.*, 2005; Honnappa *et al.*, 2009; Montenegro Gouveia *et al.*, 2010). Kif18A, in contrast, is a potent

This article was published online ahead of print in MBoC in Press (http://www.molbiolcell.org/cgi/doi/10.1091/mbc.E15-11-0803) on February 24, 2016.

*Address correspondence to: Linda Wordeman (worde@uw.edu).

Abbreviations used: BFP, blue fluorescent protein; ch-TOG, colonic and hepatic tumor overexpressed gene; EB, end-binding protein; FBS, fetal bovine serum; FKBP, FK506-binding protein; FRB, FKBP12-rapamycin–binding domain of mTOR; GFP, green fluorescent protein; IPNN, IP>NN mutant version of MCAK/Kif2C; MCAK, mitotic centromere–associated kinesin; siRNA, small interfering RNA.

suppressor of chromosome oscillations, an activity that arises from suppression of kinetochore MT dynamics (Stumpff *et al.*, 2008, 2011, 2012; Du *et al.*, 2010; Hafner *et al.*, 2014). These two motors appear to have distinguishably different activities at MT ends in vitro: MCAK/Kif2C catalytically removes tubulin dimers (Desai *et al.*, 1999; Hunter *et al.*, 2003; Wagenbach *et al.*, 2008; Cooper *et al.*, 2010), whereas Kif18A suppresses the loss and addition of dimers at MT ends (Du *et al.*, 2010; Stumpff *et al.*, 2011). Both motors are good candidates to influence MT assembly rates in cells, and both influence the length of MTs in vivo. Because cells are capable of responding to alterations in MT polymer and free dimer by raising or lowering tubulin synthesis accordingly (Gay *et al.*, 1989; Gonzalez-Garay and Cabral, 1996), we used both rapamycin-dependent rapid relocalization of the motors from MT ends to the plasma membrane (Suh *et al.*, 2006; Ufret-Vincenty *et al.*, 2011) and overnight small interfering RNA (siRNA) depletion to quantify rapid versus long-term responses in MT assembly rates to depletion of these motors.

Rapid loss of these modulators from MT ends initiated an immediate change in MT assembly rates. In mitotic spindles, astral MTs were more responsive to changes in MT assembly rates by MCAK/Kif2C and Kif18A than were the nonkinetochore spindle MTs. Rapid loss of MCAK/Kif2C resulted in an immediate increase in MT assembly rates that appeared to be rapidly compensated by lower MT nucleation rates at mitotic centrosomes. In contrast, loss of Kif18A resulted in a striking decrease in astral MT assembly rates. Slow (16–36 h) depletion of these modulators using siRNA elicited opposite effects on MT assembly rates. The diametrically opposite effect of rapid versus slow loss of kinesin regulators likely arises from correlated changes in tubulin protein levels as the cell attempts to adjust to changes in assembly kinetics that alter the concentration of free tubulin dimers. Finally, these data also help refine our understanding of both Kif18A and MCAK/Kif2C's activity in live cells. MCAK/Kif2C possesses a demonstrated ability to catalytically disassemble MTs in an ATP-dependent manner (Desai *et al.*, 1999; Hunter *et al.*, 2003; Helenius *et al.*, 2006; Cooper *et al.*, 2010) and promote MT catastrophes (Gardner *et al.*, 2011). We show that, in the cell, MCAK/Kif2C can use these activities to suppress MT assembly rates when recruited to MT tips by EB1. Similarly, in the live cell, Kif18A uses its ability to suppress MT dynamics to cap subsets of MTs within the spindle, effectively removing them from polymer/dimer partitioning. Finally, we show that a rapid increase in MT assembly rate is compensated by a decrease in MT nucleation in live cells, whereas a rapid decrease in assembly rate is not similarly compensated by an increase in MT nucleation at centrosomes. This observation can be modeled in silico when nucleation sites on the centrosome are limiting, suggesting that MT nucleation at mitotic centrosomes is maximal and limiting in mitotic cultured somatic cells. Here we establish an early framework to understand how global MT dynamics is controlled in live cells and how stable changes in MT dynamics arise in live cells in response to genetic and experimental lesions.

RESULTS

We showed previously that dual depletion of Kif4A and Kif18A rescues the Kif18A congression defect, restoring proper spindle structure and function (Stumpff *et al.*, 2012). Because both kinesins are plus end–directed motors, the distinct effect of Kif4A must be attributed to suppression of MT assembly (Bringmann *et al.*, 2004; Hu *et al.*, 2011; Stumpff *et al.*, 2012). SiRNA depletion of Kif4A leads to an increase in MT assembly rates, which antagonizes congression (Stumpff *et al.*, 2012). Using similar methodology (Figure 1A and Supplemental Movie S1), we measured MT assembly rates after overnight Kif18A and Kif2C/MCAK depletion. Of interest, siRNA

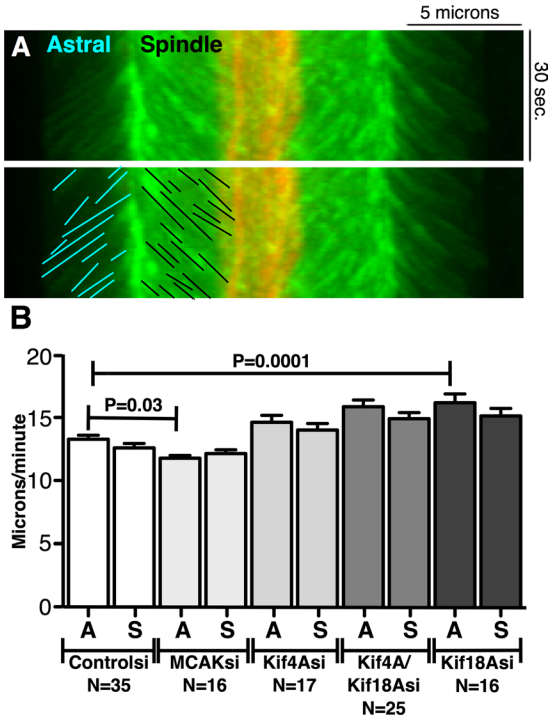

FIGURE 1: Overnight depletion of MCAK/Kif2C and Kif18A stably alters MT assembly rates. (A) Example of measurements of astral vs. spindle MT rate measurements from kymographs of EB3-GFP–expressing (green) and CENP-B-cherry–expressing (red) mitotic spindles. Astral MTs assemble toward the cell cortex, whereas spindle MTs assemble toward the chromosomes in the spindle midzone. (B) SiRNA depletion of MCAK/Kif2C decreases astral MT assembly, whereas Kif18A depletion leads to significantly increased MT assembly rates, similar to Kif4A.

depletion of MCAK/Kif2C and Kif18A significantly lowered and increased MT assembly rates in mitotic spindles, respectively (Figure 1B; $p = 0.033$ and 0.0001). This cellular effect was surprising because MCAK/Kif2C's well-documented catastrophe-promoting activity has been shown in vitro to be independent of MT assembly rates (Montenegro Gouveia *et al.*, 2010; Gardner *et al.*, 2011).

The opposite effects on MT assembly rates exhibited by these two motors was further puzzling because both have been shown to restrain MT length in live cells (Gupta *et al.*, 2006; Varga *et al.*, 2006; Rizk *et al.*, 2009, 2014; Stumpff *et al.*, 2011; Domnitz *et al.*, 2012; Su *et al.*, 2013), albeit using different mechanisms. We provisionally hypothesized that the antagonism underlying the effect of these two motors on MT turnover might underlie their opposed effect on MT assembly rates. MCAK/Kif2C, for example, was shown to increase MT turnover in kinetochore fibers (Wordeman *et al.*, 2007). Using photoactivatable green fluorescent protein (GFP)–PA-tubulin, we show here that Kif18A suppresses MT turnover in kinetochore fibers. Depletion of Kif18A significantly ($R^2 = 0.99$; $S_{x.y} = 0.01$) decreases the half-life of tubulin turnover in these kinetochore fibers (Supplemental Figure S1A). Thus in kinetochore fibers MCAK/Kif2C and Kif18A appear to manifest opposite effects on MT turnover, with MCAK/Kif2C promoting and Kif18A suppressing MT turnover.

To investigate the influence of MT end–modulating kinesins on MT assembly rates with greater temporal control than is afforded by overnight depletions using siRNA, we designed motor constructs that could be rapidly displaced from MTs to the cell membrane with rapamycin. For MCAK/Kif2C, we fused the full-length MCAK/Kif2C

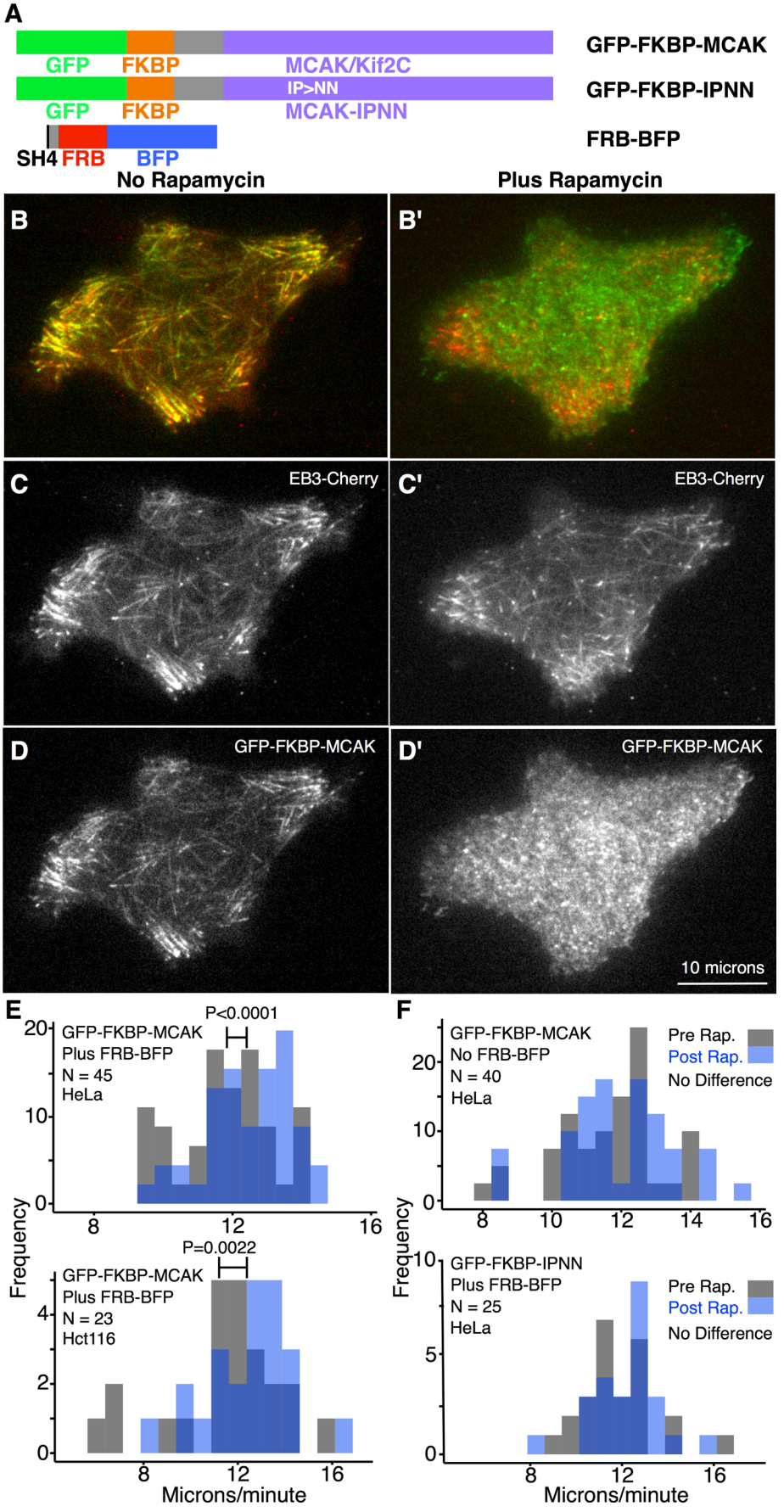

coding region to GFP-FK506–binding protein (FKBP; Suh *et al.*, 2006). The membrane-bound, rapamycin-dependent dimerization partner SH4-FKBP12-rapamycin–binding domain of mTOR (FRB) was fused to blue fluorescent protein (BFP; Figure 2A). Cultured interphase cells were triply transfected with either GFP-FKBP-MCAK or GFP-FKBP–IP>NN mutant version of MCAK/Kif2C (IPNN) and both FRB-BFP and EB3-cherry. The GFP-FKBP-IPNN construct serves as a control for effects that are specific for microtubule plus-end tracking protein (+TIP)–associated MCAK/Kif2C (Domnitz *et al.*, 2012), as this mutant is fully functional with respect to depolymerizing activity but will not associate with EB1 at MT plus ends. GFP-FKBP-MCAK localized to all subcellular regions in which full-length MCAK/Kif2C normally appears, including MT plus ends (Figure 2, B and D). The extent of MT depolymerization by GFP-FKBP-MCAK in CHO cells (Ovechkina *et al.*, 2002) was not significantly different from that in GFP-MCAK/Kif2C (unpublished data). We found that the extent and speed with which GFP-FKBP constructs relocalized to the membrane depended on robust expression levels of the SH4-FRB-BFP construct. For this reason, we limited our analysis to cells that possessed high levels of SH4-FRB-BFP. Because FRB-BFP was highly subject to bleaching, it could not be consistently imaged or quantified, only rapidly evaluated by eye. Cells possessing

FIGURE 2: Relocalization of MCAK/Kif2C from MT ends raises MT assembly rates. (A) GFP-FKBP fused either to MCAK/Kif2C or MCAK-IPNN, which does not interact with EB1 at MT ends. Membrane-localizing SH4-FRB was linked to BFP to identify triply transfected cells. (B, B′) Total internal reflection fluorescence microscopy of GFP-FKBP-MCAK (green) and EB3-cherry (red) before (B) and after (B′) rapamycin addition. (C, C′) EB3-cherry before (C) and after (C′) rapamycin addition. (D, D′) GFP-FKBP-MCAK before (D) and after (D′) rapamycin triggers the relocalization of GFP-FKBP-MCAK to the membrane. (E) MT assembly rates significantly increase ($p < 0.0001$ and 0.0022) after rapamycin-induced GFP-FKBP-MCAK relocalization to the plasma membrane. HeLa and Hct116 cells (top, bottom). (F) An increase in MTs assembly rates is not evident without the plasma membrane–bound partner (top, no GFP-FKBP-MCAK relocalization) or in the absence of the association of MCAK/Kif2C with EB1 (GFP-FKBP-IPNN). Black, before rapamycin addition; blue, 1–5 min after rapamycin.

strong SH4-FRB-BFP fluorescence were imaged in the GFP/red fluorescent protein (RFP) filters and marked for position on the microscope stage. Microtubule assembly rates (via EB3-RFP) were imaged rapidly for 30 s. Between 5 and 10 min after application of rapamycin, cells were revisited in order, point by point, by position on the stage. Cells were reimaged in the GFP/RFP filters and scored for relocalization. Only those cells that exhibited 50–100% relocalization of GFP-FKBP-MCAK were reimaged for MT assembly rates. Examples of cells quantified for GFP-FKBP relocalization are shown in Supplemental Figure S1B. When GFP-FKBP-MCAK rapidly relocalized to the plasma cell membrane (Figure 2, B′ and D′) upon administration of rapamycin, the mean rate of MT assembly significantly increased from 11.8 ± 0.2 (SEM) to 12.5 ± 0.18 (SEM) μm/min in HeLa cells (Figure 2E, $p < 0.0001$). We obtained a similar result in interphase Hct116 cells: an increase in MT assembly rate from 11.4 ± 0.4 (SEM) to 12.5 ± 0.4 (SEM) μm/min after rapamycin administration (Figure 2E; $p = 0.0022$). Rapamycin-treated cells lacking SH4-FRB-BFP (Figure 2F, top) or expressing GFP-FKBP-IPNN instead of GFP-FKBP-MCAK (Figure 2F, bottom) did not exhibit significantly increased MT assembly rates. This suggests that +TIP-bound MCAK/Kif2C suppresses MT assembly rates in live cells. We further tested this finding using an alternate method of rapid MCAK/Kif2C depletion. We constructed an MCAK/Kif2C degron that will rapidly degrade upon administration of auxin. We were not able to test this construct on mitotic cells because the transfection efficiency of the construct was poor. However, in interphase cells, we found that increased MT assembly rates were observed by 30 min after application of auxin (Supplemental Figure S1C). We were surprised to observe that MT assembly rates increased upon rapid relocalization of MCAK/Kif2C, a result that does not phenocopy the lowered MT assembly rates observed after siRNA depletion.

Because the effects of siRNA depletion were measured on live mitotic spindles, we examined whether rapid relocalization of GFP-FKBP-MCAK from mitotic spindles also promoted increased MT assembly rates, similar to what we saw in interphase cells. We used rapamycin to rapidly relocalize GFP-FKBP-MCAK from the mitotic spindle to the plasma membrane in mitotic cells (Figure 3, A–A″, and Supplemental Movie S2). Only the region of MT elongation proximal to the centrosome was used in the measurements to avoid any possibility that the assembling MT plus ends were encountering membrane-bound motor. Similar to the result in interphase cells, we found that relocalization of GFP-FKBP-MCAK away from the spindle resulted in a significant increase in astral MT assembly rates relative to spindle MTs (Figure 3B, blue boxes marked A). In mitotic spindles, as opposed to interphase cells, MCAK/Kif2C appears to exert its effect preferentially on astral MT arrays, possibly reflecting a different spatial regulatory environment of these two subsets of nonkinetochore MTs (Rizk *et al.*, 2009).

To investigate whether Kif18A and MCAK/Kif2C manifest similarly opposite effects on nonkinetochore MT assembly rates in spindles, we prepared GFP-FKBP-Kif18A constructs (Figure 4A) to assay for rapid changes in MT assembly upon relocalization of GFP-FKBP-Kif18A to the plasma membrane (Figure 4B). We observed a striking reduction in astral MT assembly rates when GFP-FKBP-KIf18A was rapidly depleted from the mitotic spindle (Figure 4C, right; $p = 0.0014$). In summary, rapid loss of GFP-FKBP-MCAK increase astral MT assembly rates, whereas rapid loss of GFP-FKBP-Kif18A decreases astral MT assembly rates. This does not phenocopy the effect of slow depletion of these motors using siRNA. Instead, it represents an opposite response relative to those data (summarized in Figure 5).

When MT assembly rates increase rapidly, as they do during rapamycin-induced GFP-FKBP-MCAK relocalization, it is unclear how

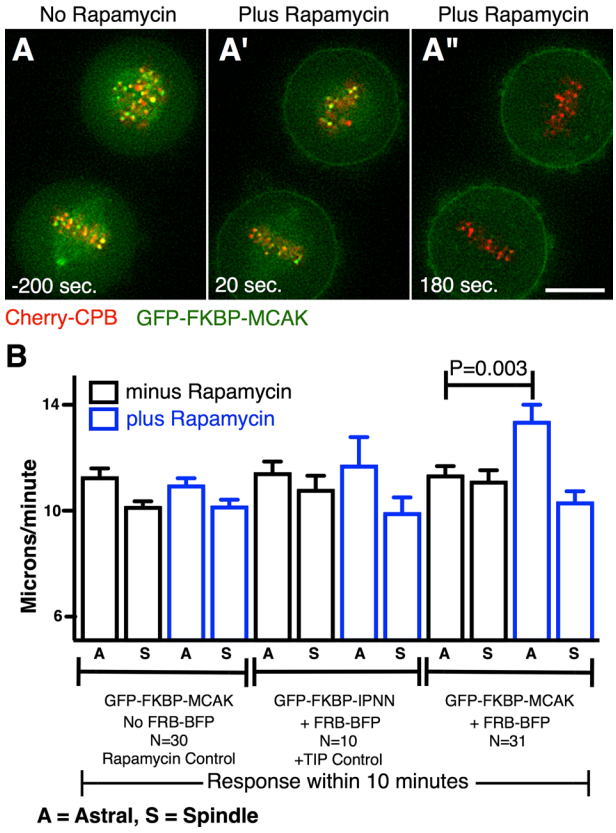

FIGURE 3: Relocalization of MCAK/Kif2C from MT ends in mitotic spindles raises astral MT assembly rates. (A–A″) GFP-FKBP-MCAK relocalization occurs within 3 min after rapamycin addition. (B) Astral (A) and spindles (S) MT assembly rates measured in mitotic cells expressing EB3-cherry, GFP-FKBP-MCAK, and FRP-BFP before (black) and after (blue) rapamycin relocalization. Only GFP-FKBP-MCAK plus FRP-BFP exhibits a significant ($p = 0.003$) increase in astral MT assembly rates.

this is accommodated unless MT polymer is compromised elsewhere. The simplest hypothesis to test is that MT nucleation off of centrosomes is inhibited when assembly rates are increased and promoted when MT assembly rates are decreased. Relative MT nucleation events within a short timeframe and limited spatial distribution were quantified from images collected at 3 frames/s at a single plane of focus (diagrammed in Figure 6A). When relative MT nucleation rates were measured at mitotic spindle poles before and after instantaneous GFP-FKBP-MCAK relocalization, nucleation rates were found to have decreased under conditions in which rates of assembly at MT plus ends increased (Figure 6B). Surprisingly, rapid relocalization of Kif18A did not alter (or increase) MT nucleation rates (Figure 6C) as one might predict based on the decreased nucleation rates seen when MT assembly rates are increased. It might be that in cultured mammalian somatic cells, MT nucleation sites are limiting or fully occupied. It was further surprising to find that long-term siRNA depletion of both MCAK/Kif2C and Kif18A revealed no significant alterations in nucleation capacity (Figure 6D). This suggested that the 16-h depletion time associated with siRNA depletion enabled the cell to accommodate to changes in MT assembly rates to maintain consistent rates of MT nucleation and full occupancy of all centrosomal MT nucleation sites.

If there is an inverse relationship between a rapid increase in MT assembly rates and lower MT nucleation, why is this relationship

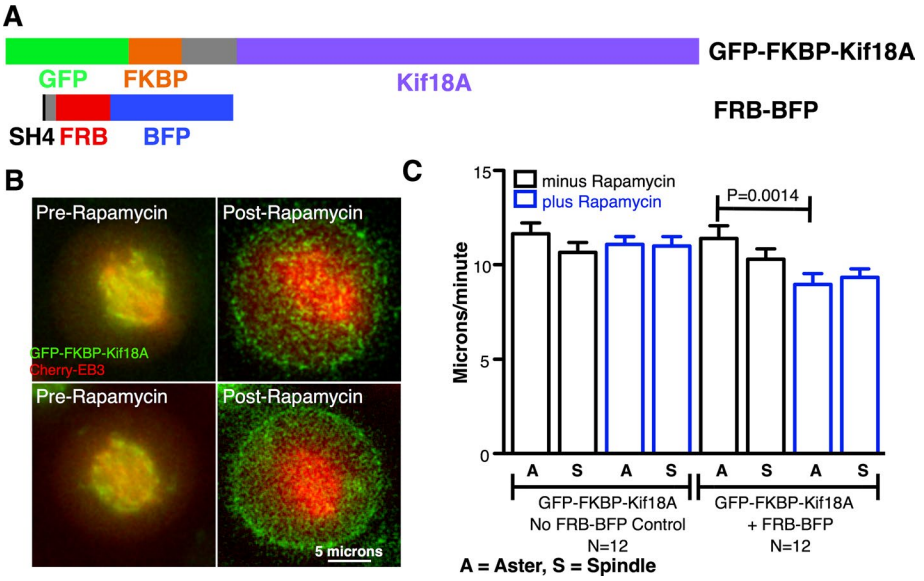

FIGURE 4: Rapid loss of Kif18A from mitotic spindles decreases MT assembly rates. (A) Constructs used to rapidly remove Kif18A from mitotic spindles. (B) Examples of live mitotic spindles expressing GFP-FKBP-Kif18A (green) and EB3-cherry (red) before (left) and after (right) rapamycin-dependent relocalization of GFP-FKBP-Kif18A to the plasma membrane. (C) Relocalization of GFP-FKBP-Kif18A to the plasma membrane results in a significant ($p = 0.0014$) decrease in astral MT assembly rates, which is not evident in rapamycin-treated cells, which do not possess the FRB-BFP membrane localization partner.

invalidated both when rates are decreased and also when regulators are slowly depleted by siRNA? One possible explanation for the latter effect is that over a longer time course, the tubulin autoregulatory system responds to siRNA treatment in an attempt to normalize the concentration of free tubulin dimer. To test this hypothesis, we quantified β-tubulin I (TUBB) protein level and also α-tubulin after MCAK/Kif2C and Kif18A depletion. Depletion of both MCAK/Kif2C and Kif18A correlated with an increase in TUBB and α-tubulin protein levels (Figure 7A). Because colonic and hepatic tumor overexpressed gene (ch-TOG) has also been implicated in controlling MT assembly rates (Cassimeris *et al.*, 2009; Ertych *et al.*, 2014), we analyzed ch-TOG protein levels on the same blots along with TUBB. We found that, instead of being correlated with conditions that increase MT assembly rates, the level of ch-TOG changed over time commensurate with the level of TUBB protein (unpublished data). We hypothesize that an increase in cytoplasmic free tubulin dimer concentration rescues MT nucleation at the centrosome.

Raising cytoplasmic tubulin levels via tubulin synthesis takes time. For this reason, it is difficult to test experimentally the hypothesis that a rapid increase in MT assembly rates compromises centrosomal MT nucleation and that this effect can be rescued by increasing the cytoplasmic level of tubulin. However, one can test this hypothesis in silico using programs that model MT dynamics. We used Skeledyne, a three-dimensional force-based simulator of cytoskeletal dynamics, to test our hypothesis. The source code is available at http://rusty.fhl.washington.edu/celldynamics/downloads/simcode.html. The program is capable of scoring both the number of MTs and the number of centrosomal MTs in real time during the simulation. Furthermore, the assembly rates and GTP-tubulin levels can be increased or decreased during the simulation and the effect on centrosomal MT numbers scored. Figure 7, B and C, shows, respectively, identical points in the simulation run with default MT assembly rates (Figure 7B) or assembly rates that are increased by an average of 30% (Figure 7C). Figure 7, D and E, shows the time course of MT assembly under the same two conditions for 10 simulations. Note that the total number of centrosomal MTs plateaus at a lower number when the MT assembly rate is higher (Figure 7, D vs. E, red traces). An interruption in the MT behavior occurs early in the simulation when the MTs encounter the cell edge (Figure 7, D and E, asterisk). This is similar to MT behavior in live cells when they encounter resistance at the edge of the cell. Figure 7F shows the change in centrosomal MT number when the assembly rates are switched from low to high at a point 20 min into the simulation. The box-and-whisker plot on the left shows the decrease in centrosomal MTs before and after a 30% increase in MT assembly rates. The mean difference in centrosomal MTs for 10 simulations is –27 MTs ± 6 (SEM). In contrast, when MT assembly rates are increased in conjunction with an increase in GTP-tubulin, the mean loss in MT number is decreased by more than half (Figure 7F, right). The plots of the two groups of simulations are shown in Supplemental Figure S2, A and B. Simulations in MT dynamics support our hypothesis that increased MT assembly rates in a system in which tubulin levels are

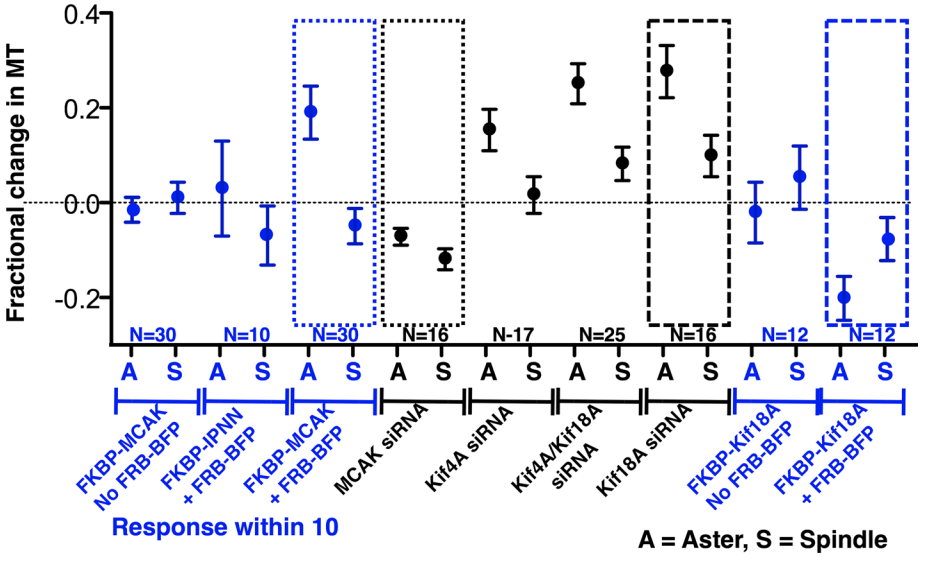

FIGURE 5: Overnight depletion of MCAK/Kif2C and Kif18A does not phenocopy rapid relocalization. Summary of the normalized changes in MT assembly rates for mitotic asters and spindles relative to control measurements for each experiment. The response of MT assembly rates to rapid loss MCAK/Kif2C or Kif18A (blue dashed boxes) is the opposite of the response to slow depletion (black dashed boxes).

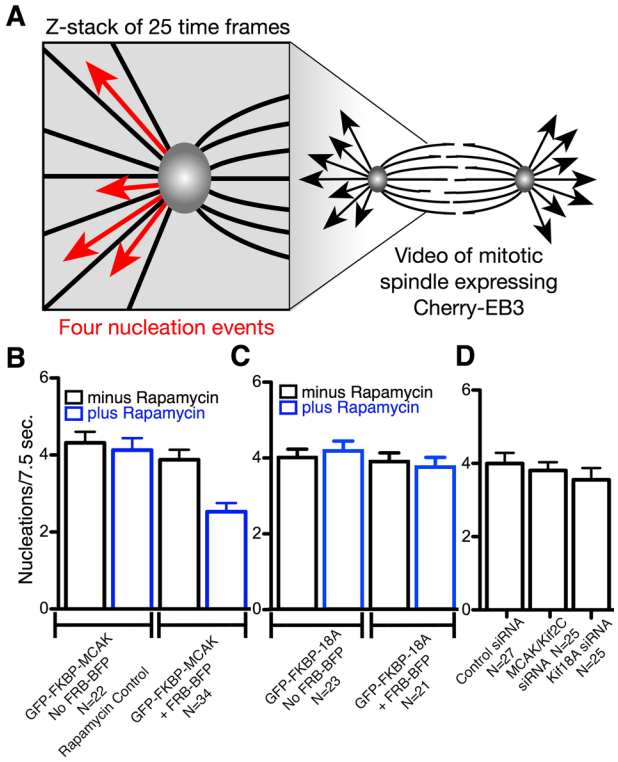

FIGURE 6: Increased MT assembly rates are compensated by reduced MT nucleation. (A) Newly nucleated MTs were quantified in a *Z*-stack of a defined number of time points. (B) Rapid removal of GFP-FKBP-MCAK correlated with lower MT nucleation rates ($p = 0.0002$). (C) Rapid removal of GFP-FKBP-Kif18A did not significantly change MT nucleation. (D) MT nucleation rates in MCAK/KIf2C and Kif18A siRNA–depleted cells were not significantly different from control siRNA–treated cells. Thus slow depletion of MT regulators did not compromise centrosomal nucleation capacity.

held constant will reduce the number of centrosomal MTs. Furthermore, the modeling also supports the idea that MT nucleation can be rescued in the face of raised MT assembly if GTP-tubulin levels are also increased during the transition.

To explore the effect of reduced MT assembly rates on nucleation, we ran eight simulations with MT assembly rates reduced by 30% (Figure 8A). We found that, unlike our experimental data, the number of centrosomal MTs was increased. In fact, when the number of possible nucleation sites is not limiting, curves fitted to the simulations indicate that the number of centrosomal MTs and the assembly rate exhibit a dose-dependent inverse correlation (Figure 8B). This suggested the possibility that in live mitotic cells, centrosomal nucleation capacity may be limiting and nucleation sites fully occupied. In support of this hypothesis, limiting the number of nucleation sites per centrosome (Figure 8C, dotted lines, and Supplemental Figure S2, C and D) reflected our experimental data more closely. When nucleation sites are limiting, reduced MT assembly rates did not increase nucleation, whereas increased MT assembly rates still increased nucleation as observed when nucleation sites are not limiting.

Skeledyne is not presently configured to handle MT-capping proteins. For this reason, we cannot at present model the behavior of Kif18A. However, given that we found that both Kif2C/MCAK and Kif18A suppress MT assembly in live cells, it is likely that the opposite effects of these two regulators on MT assembly rates are attributable to the differential spatial activity of the two motors. MCAK/Kif2C is recruited to all assembling MTs via EB1, whereas Kif18A's high processivity amplifies its activity to subsets of MTs with higher stability (Stumpff *et al.*, 2011). Thus both the time course of experimental treatment (longer treatments triggering cellular compensation) and the inherent spatial distribution of regulators on subsets of MTs govern the experimental quantification of cellular MT dynamics. This idea is illustrated in Figure 8, D and E, for rapid and long-term depletion of MT-end regulators Kif2C/MCAK and Kif18A.

DISCUSSION

Overexpression of MCAK/Kif2C over the course of 16–24 h suppresses tubulin synthesis (Ovechkina *et al.*, 2002; Montenegro Gouveia *et al.*, 2010; Domnitz *et al.*, 2012). This is because this kinesin uses its ATPase activity to remove tubulin dimers from MT ends. The increase in free tubulin suppresses further tubulin synthesis by destabilizing tubulin mRNA (Gay *et al.*, 1987; Pachter *et al.*, 1987; Yen *et al.*, 1988). For this reason, it was not surprising to discover that long-term MCAK/Kif2C depletion by siRNA leads to increased tubulin synthesis commensurate with increased sequestration of free tubulin as polymer. It was surprising, however, to discover that rapid loss of MCAK/Kif2C from MT plus ends removes MT growth-suppressing activity, leading to an increase in MT assembly rates. This was surprising because MCAK/Kif2C's well-documented catastrophe-promoting activity has been shown in vitro, by a number of thorough and well-executed studies, to be independent of MT assembly rates (Montenegro Gouveia *et al.*, 2010; Gardner *et al.*, 2011). We hypothesize that MCAK/Kif2C suppresses MT assembly at normal cellular concentrations by intermittent removal of dimers from the MT end. This hypothesis is based on a large body of work that demonstrates unambiguously that MCAK/Kif2C removes tubulin from MT ends in a mildly processive and ATP-dependent manner (Desai *et al.*, 1999; Hunter *et al.*, 2003; Helenius *et al.*, 2006; Wagenbach *et al.*, 2008; Cooper *et al.*, 2010). In the context of the live cell, catastrophe activity may be suppressed by other MT plus end–associated regulators, leading to MCAK/Kif2C's primary cellular activity manifesting as suppression of MT assembly.

The increase in MT assembly rates seen during rapid relocalization of MCAK/Kif2C cannot be sustained without the sacrifice of polymer to reduce the number of MT plus ends. Accordingly, we observed that cells exhibit decreased nucleation from the centrosome after rapid MCAK/Kif2C loss from MT ends (Figure 6B; illustrated in Figure 8D). However, on a longer time scale, this increased flux of free tubulin into polymer stimulates tubulin synthesis (Figure 7A). Increased tubulin synthesis, over time, may be able to fulfill the nucleation capacity of the centrosome to restore the number of free MT ends available in the cell. Of interest, tubulin synthesis does not perfectly reestablish previously observed control MT assembly rates but instead consistently settles at a lower overall MT assembly rate. We do not know why this occurs but assume that increased tubulin synthesis does not fully restore wild-type tubulin dimer levels in the absence of MCAK/Kif2C's catastrophe and depolymerase activities. Of importance, however, we cannot assume that MCAK promotes MT growth based on the lowered rates of MT assembly, because the cell has compensated for MCAK/KIf2C loss and complicated the interpretation of MCAK/Kif2C's cellular activity. This illustrates the hazard of ascribing activities to MT regulators based solely on siRNA depletion.

A similar increase in TUBB protein level is observed after slow Kif18A depletion. Unlike MCAK/Kif2C, mammalian Kif18A has been shown to suppress (rather than promote) MT dynamics and assembly in live cells and in vitro (Gupta *et al.*, 2006; Du *et al.*, 2010; Stumpff *et al.*, 2011). An important difference between MCAK/Kif2C's growth suppression and Kif18A's MT growth suppression is that the high processivity associated with Kif18A amplifies its

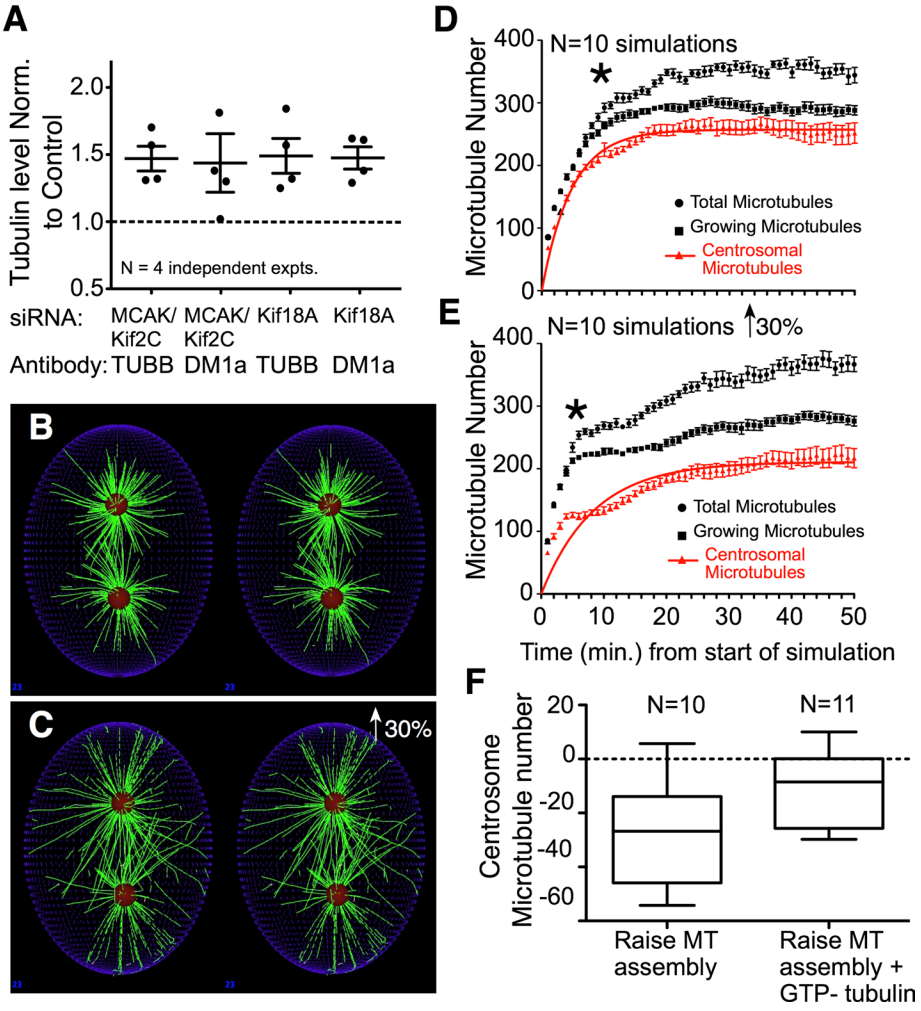

FIGURE 7: Tubulin synthesis rescues nucleation changes associated with increased MT assembly rates. (A) MCAK/Kif2C and Kif18A depletion leads to an increase in TUBB protein and α-tubulin. Error bars are SEM. (B) MT assembly simulated for 10 min using Skeledyne. (C) Increased rates of MT assembly simulated for 10 min. (D) Ten simulations with identical parameters set as in B. Centrosomal MT numbers plateau after 20 min. (E) Ten simulations in which parameters are identical to C. Centrosomal MTs plateau at a lower number than in D, suggesting that higher MT assembly rates compromise nucleation. (F) Compiled simulations in which MT assembly rates are raised instantaneously after 20 min with and without added GTP-tubulin. Box represents minimum to maximum measurement of the change in MT number. Added tubulin rescues the loss of centrosomal MTs seen when the rate of assembly is increased.

accumulation on stable subsets of spindle MTs (Stumpff *et al.*, 2008; Masuda *et al.*, 2011; Weaver *et al.*, 2011; Rizk *et al.*, 2014). This represents a key distinction between these two classes of motors. MCAK/Kif2C has the potential to influence a majority of the MT plus ends in the cell, as it associates with all of them via EB1. In contrast, Kif18A is recruited preferentially to less dynamic subsets of MTs, where it further suppresses assembly and disassembly, thus amplifying the stabilization of these MTs. For this reason, the loss of Kif18A is more analogous to the depletion of a capping protein, which increases the number of free MT ends available in the cellular milieu (illustrated in Figure 7B). Increased numbers of MT ends compete for existing free tubulin dimers, slowing the global MT assembly rates while also reducing the tubulin dimer concentration. This should also lead to a long-term increase in tubulin synthesis, which we confirmed experimentally (Figure 7A). Although our simulations indicate that decreased MT assembly rates can increase nucleation rates, we find experimentally that nucleation does not increase when Kif18A is rapidly relocalized. We hypothesize this is because the new free MT ends compete for tubulin dimers and prevent a measureable increase in nucleation (Figure 8E). An alternative explanation, which is also supported by our simulations, is that MT nucleation is already maximally occupying all available centrosomal nucleation sites and cannot further increase. If that were the case, it would be unique to somatic cells, as increased MT nucleation has been achieved in early divisions of *Caenorhabditis elegans* eggs (Srayko *et al.*, 2005) by RNA interference depletion of regulators. This is an interesting area for further study.

The response of MTs to changes in the activity of regulators is influenced by the concentration of free assembly–competent tubulin, the concentration of MT ends, the nucleation capacity of the centrosome (Zhou *et al.*, 2002), and possibly other regions of cellular MT assembly (Chabin-Brion *et al.*, 2001; Grimaldi *et al.*, 2013). In live mammalian cells, it is extremely difficult, if not impossible, to measure the total number of MTs and thus the concentration of free MT ends. Note that, for technical reasons, it is also difficult to unambiguously quantify these bulk parameters in in vitro microscopic assays. It is also relatively difficult to quantify small changes in polymer-to-dimer ratios in cells. However, it is relatively easy to measure MT assembly rates and, with greater difficulty, relative nucleation capacity in cells. Our data underscore that MT behavior is answerable to steady-state dynamic instability in the short term and tubulin autoregulation over time. As a result, the phenotypes characterized from siRNA depletion do not necessarily phenocopy those measured by instantaneous depletion, although both techniques are useful when their limitations are understood.

Although at present it is impossible to quantify centrosomal MTs in live mitotic spindles it is possible to model MT assembly in silico under conditions in which MT number, length, and centrosomal association can be known. We tested our hypotheses using Skeledyne, a computer program that models MT assembly while tracking the diffusion and convection of soluble factors throughout the cell's cytoplasm (Odell and Foe, 2008). This computer simulation models the variations in MT assembly states that are observed when MTs encounter cytoplasmic domains and the cell cortex. We found that, in this closed model system, when MT assembly rates are increased, fewer centrosomal MTs are assembled, to compensate for the increased rate of overall MT assembly (Figure 7, D and E). Furthermore, we found that an instantaneous increase in MT assembly rates leads to a similarly rapid decrease in centrosomal MTs in the model, which was rescued when the rate of assembly and proportion of GTP-tubulin were increased together (Figure 7F). At present, such computer simulations offer the best chance to test our interpretations of empirical data.

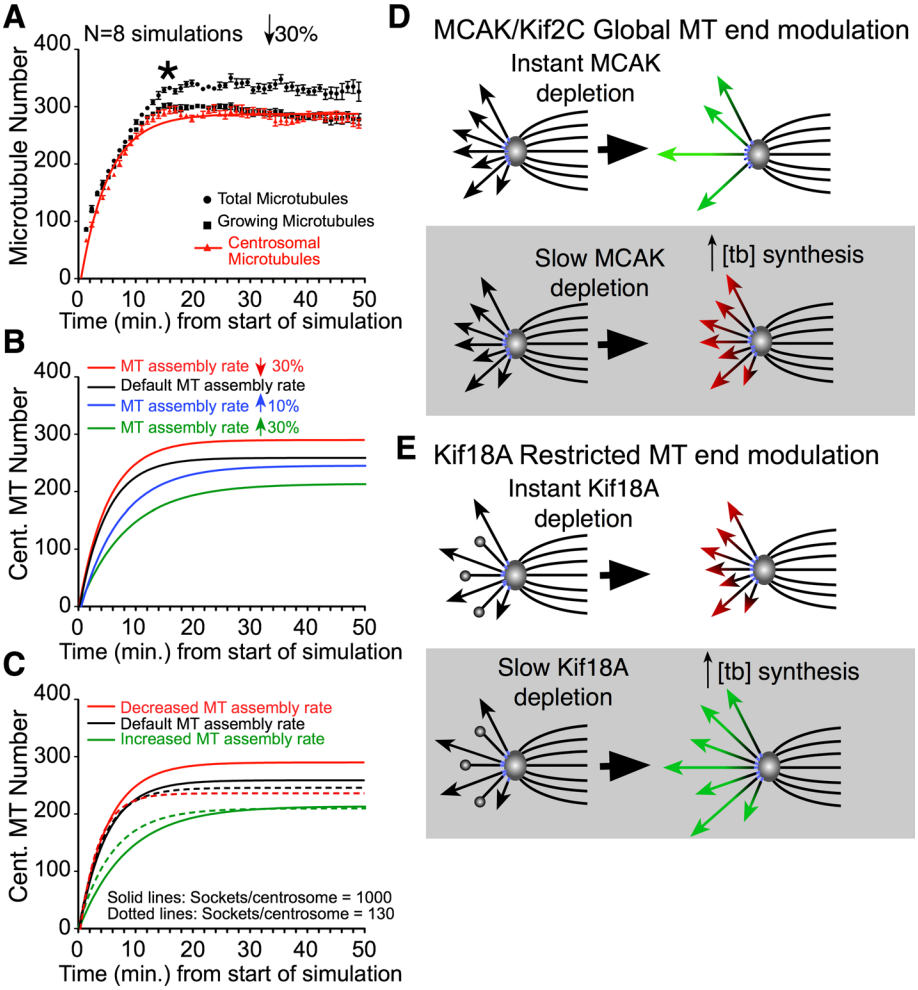

FIGURE 8: Simulations predict a dose-dependent relationship between assembly rates and nucleation capacity. (A) Reduced MT assembly rates increase the number of centrosomal MTs. (B) Curve fits of centrosomal MT numbers from simulations run at different MT assembly rates suggest a dose-dependent relationship between assembly rates and centrosome MTs when nucleation sockets are not limiting. (C) Limiting the number of available sockets for nucleation eliminates the increased nucleation seen when MT assembly rates are reduced. (D) MCAK/Kif2C suppresses MT assembly rates in live cells. Loss of MCAK/Kif2C drives more tubulin dimer into polymer, stimulates tubulin synthesis, and compromises centrosomal MT nucleation. This effect on nucleation is compensated by tubulin autoregulation. (E) Kif18A caps a subset of MT ends within the spindle. Loss of Kif18A increases the concentration of free MT ends, leading to depletion of free tubulin and stimulation of tubulin synthesis but no change in nucleation capacity. Black arrows, assembling MTs; red arrows, slower-assembling MTs; green arrows, faster-assembling MTs.

In conclusion, our data both refine our understanding of the contribution that MCAK/Kif2C and Kif18A make to MT assembly regulation in live cells and also illustrate the risk inherent in absolute reliance on long-term alterations of MT regulators to understand molecular function. MCAK/Kif2C and Kif18A both appear to restrict MT length in live cells (Stumpff *et al.*, 2008; Du *et al.*, 2010; Weaver *et al.*, 2011; Domnitz *et al.*, 2012). Whereas MCAK/Kif2C is a potent depolymerizer of MTs (Hunter *et al.*, 2003; Helenius *et al.*, 2006; Cooper *et al.*, 2010), its major role at free MT plus ends within cells appears to be to restrict MT length by suppressing MT assembly rates. This might involve other +TIP cellular proteins because this activity has not been seen in a number of in vitro assays (Montenegro Gouveia *et al.*, 2010; Gardner *et al.*, 2011). Ironically, however, alterations in the levels of these two MT regulators exhibit inverse effects on MT assembly rates in cells. We believe that this can be explained by differences in the spatial distribution of these proteins in cells and exactly how the full complement of MTs in the cell responds to this spatial incoherence.

MCAK/Kif2C associates with MT plus ends in an EB1-dependent manner, and so this activity has the potential to manifest at all EB1-decorated MT ends. For this reason, loss of MCAK/Kif2C has the potential to affect all MTs simultaneously, enabling them to assemble more rapidly. Kif18A also suppresses MT growth in vitro and in live cells, with the important caveat that its processive motility enables it to selectively suppress, and even halt, the growth of the less dynamic proportion of the MTs within a bulk population of dynamic MTs (Du *et al.*, 2010; Masuda *et al.*, 2011; Weaver *et al.*, 2011). When this motor is rapidly depleted, new MT ends that were previously not available to attract tubulin dimers are uncapped. This might globally reduce MT assembly rates at all other dynamic MT ends by increasing the concentration of new assembly-competent MT plus-ends. To complicate the story, overnight depletion of both of these two regulators using siRNA stimulates the cell to synthesize tubulin. This changes the microtubule dynamic parameters by increasing the concentration of tubulin in the cell in conjunction with loss of the regulator. Thus the assignment of molecular activities based on changes to MT assembly parameters from experimental manipulations of MT regulators must be evaluated against this cellular backdrop. Accordingly, the refinement of MT dynamics by MT regulators in cells is likely to be similarly distinct from the direct activities measured by in vitro studies.

MATERIALS AND METHODS

cDNA and siRNA constructs

SBFP2 was inserted into LDR-FRB-pcDNA3 (Inoue *et al.*, 2005) to express plasma membrane-associated Lyn11-FRB-SBFP2. FRB's binding partner, FKBP, was inserted into plasmids derived from pEGFP-C1 encoding Kif2C, Kif4, or Kif18A to express EGFP-FKBP-kinesin. Each kinesin gene had been altered previously by silent mutation to resist its specific siRNA. Rapamycin (Sigma-Aldrich, St. Louis, MO) was added during filming to culture medium to induce binding of FKBP to FRB.

Kinesins were targeted for siRNA-mediated depletion using Silencer Validated siRNAs (Ambion/Life Technologies, Grand Island, NY) against Kif18A (GCCAAUUCUUCGUAGUUUUTT or GCUGGAUUUCAUAAAGUGGTT) and Kif4A (CCAAUGUGCUCAGACGUAATT or CCAAAUCAUUUGCCGAG). Control siRNA cells were treated with Silencer Negative Control#1 siRNA (Ambion/Life Technologies). MCAK/Kif2C was depleted with siRNA (s21665; Applied Biosystems). EB3-GFP (Stepanova *et al.*, 2003) and EB3-cherry were

prepared by PCR from EB3–monomeric RFP (a kind gift of Anna Akhmanova, Utrecht University, Utrecht, Netherlands). GFP–ch-TOG (Charrasse *et al.*, 1998) was a kind gift of Christian Larroque (INSERM, Montpellier, France).

MCAK/KIf2C degron

Our auxin-induced protein degradation system was based on pAID1.1-N (Cosmo Bio, Carlsbad, CA). Due to poor GFP-MCAK expression from internal ribosome entry site (IRES)–directed synthesis in pAID1.1, we constructed a two-plasmid variant. The IRES and auxin-induced degron in pAID1.1-N were replaced with SBFP2 fused to the 3′ end of TIR (pMX1535) to provide TIR activity in-*trans*, as verified by SBFP2 fluorescence. Degron-EGFP (pMX1538) and degron-EGFP-MCAK (MCAK with silent mutations to resist siRNA; pMX1542) expression vectors were constructed in pEGFP-C1, with silent mutations in the degron sequence to reduce predicted mRNA secondary structure between the 5′ untranslated sequence and degron open reading frame. Cultured cells were cotransfected with anti-MCAK siRNA, pMX1535 and either the degron-EGFP or degron-EGFP-MCAK vector, with 20 mM auxin (Sigma-Aldrich) subsequently added to induce protein degradation. Cells were imaged before and 2 h after the application of auxin.

Cell culture and transfections

Both HeLa and Hct116 cells were cultured in RPMI1640 (Gibco/Thermo Fisher, Waltham, MA) plus 10% fetal bovine serum (FBS; Hyclone/GE Healthcare, Logan, UT) and penicillin/streptomycin at 37°C and 5% CO_2. Before imaging, cells were transferred to CO_2-independent medium plus 10% FBS. For DNA transfections, cells were electroporated in a Nucleofector II (Lonza Basel, Switzerland) according to the manufacturer's instructions. GFP-FKBP-MCAK and GFP-FKBP-18A were cotransfected with siRNA directed at the respective endogenous kinesins in order to minimize any cellular response to motor overexpression and also to maximize the proportion of motor susceptible to relocalization. After transfection, cells were plated onto poly-L-lysine–coated MatTek (MatTek Corp., Ashland, MA) dishes for live imaging. When used in isolation, siRNAs complexed with Lipofectamine RNAiMAX were added according to the manufacturer's instructions (Invitrogen /Thermo Fisher, Waltham, MA). Each siRNA was used at a final concentration of 20 nM. Combinations of siRNAs were added to a final concentration of 20 nM. For TUBB and DM1a blots, cells were treated with siRNA at 20 nM. Antibodies are described in detail later.

Live imaging

Cells were imaged with a DeltaVision system (GE Healthcare, Issaquah, WA) equipped with a CoolSNAP HQCCD camera (Photometrics,Tucson, AZ), Softworx software (Applied Precision/GE Healthcare, Issaquah, WA), and a 60×/1.42 numerical aperture objective (Olympus Tokyo, Japan). Images were collected at 3 frames/s at a single focal plane for 15 s. For rapamycin-treated cells, 10 cells at a time were imaged and point marked, 1 μM rapamycin was added (Ufret-Vincenty *et al.*, 2011), and the same cells were reimaged, in order, 5 min after rapamycin. A preliminary snapshot was collected for each cell before and after rapamycin treatment to evaluate the rapamycin-induced relocalization. EB3 tracks from interphase cells were hand-tracked from the center of the cell, avoiding the extreme cell edges, or tracked using Trackmate (Fiji; Schindelin *et al.*, 2012) and filtering out of cell edges, which would be enriched with relocalized motor. Mitotic EB3 tracks were measured as described previously (Stumpff *et al.*, 2012). Baseline MT assembly rates for all controls are compared in Supplemental Figure S1D. Nucleation events were scored by assembling a *Z*-stack of 7.5-s images in one plane of the centrosome. New tracks that appeared and translocated from the centrosome within that time frame were counted. For technical reasons, no tracks entering the spindle were counted; only those in a 180° arc on the astral side of the centrosome were scored.

Statistics

Rate measurements from rapamycin-treated cells were compared before and after rapamycin addition, and significant changes were scored using paired *t* tests in Prism 5.0 (GraphPad Software, La Jolla, CA). Histograms were plotted using R. The SiRNA-treated cells were compared with control siRNA-treated cells using unpaired *t* tests (Prism 5.0). Data were also scored for variances, but there were no significantly different variances between compared data groups.

Western blot analysis of tubulin expression

CHO cells transfected with siRNA (Ambion/ Life Technologies) using RNAiMAX (Life Technologies, Grand Island, NY) were washed with phosphate-buffered saline and lysed in lysis buffer (100 mM NaCl, 50 mM imidazole-HCl, pH 7.0, 3 mM $MgCl_2$, 2 mM $CaCl_2$, 1 mM ethylene glycol tetraacetic acid, 0.5% Triton X-100, 1× Halt protease inhibitors [Thermo Fisher, Waltham, MA], 2 mM phenylmethylsulfonyl fluoride, 20 μg/ml DNaseI), scraped off plates, mixed with one-fifth volume of 6× SDS/dithiothreitol sample buffer, and heated to 70°C for 10 min. Samples were run on 4–12% gels (Novex/Thermo Fisher, Waltham, MA), blotted overnight at 42 mA to nitrocellulose membranes (Schleicher and Schuell/Sigma-Aldrich, St. Louis, MO), stained with Ponceau S (Sigma-Aldrich), and scanned. Filters were blocked with 1% BSA (Jackson Immunoresearch, West Grove, PA) for >30 min, incubated in primary antibodies against tubulin (WH0203068M4 or T6199; Sigma-Aldrich), glyceraldehyde-3-phosphate dehydrogenase (CB2002; Calbiochem, San Diego, CA), or Tog (ab86073; Abcam, Cambridge, MA), and stained with Dylight 488 donkey anti-mouse or Alexa 568 donkey anti-rabbit (Jackson Immunoresearch). Blot images were collected in a FluorChemM (ProteinSimple, San Jose, CA). Peak areas from images were calculated with ImageJ (National Institutes of Health, Bethesda, MD).

In silico simulations of MT assembly

Skeledyne was downloaded from http://rusty.fhl.washington.edu/celldynamics/downloads/simcode.html. This force-based three-dimensional simulation uses Lagrangian "cytoplasmic domains" to keep track of the diffusion and convection of soluble factors throughout a cell's cytoplasm. The cell cortex serves as a nondeformable boundary. The simulations were run on a MacBook Pro 2.6-GHz OS 10.10.5 with 16 GB of memory. Default parameters were used, except as listed in Supplemental Table S1. Screenshots of the simulation were taken each minute to record the changes in MT number and length throughout the simulation. Supplemental Movies S3 and S4 show a simulation recorded under conditions of low MT assembly versus 30% higher MT assembly.

ACKNOWLEDGMENTS

We are grateful to Sharona Gordon for the FRB and FKBP constructs. This study was supported by National Science Foundation Grant 1041173 and National Institutes of Health Grant GM69429 to L.W. and National Institutes of Health Fellowship F32GM105099 and American Cancer Society Fellowship PF1409901CCG to J.D.

REFERENCES

Bringmann H, Skiniotis G, Spilker A, Kandels-Lewis S, Vernos I, Surrey T (2004). A kinesin-like motor inhibits microtubule dynamic instability. Science 303, 1519–1522.

Cassimeris L, Becker B, Carney B (2009). TOGp regulates microtubule assembly and density during mitosis and contributes to chromosome directional instability. Cell Motil Cytoskeleton 66, 535–545.

Chabin-Brion K, Marceiller J, Perez F, Settegrana C, Drechou A, Durand G, Pous C (2001). The Golgi complex is a microtubule-organizing organelle. Mol Biol Cell 12, 2047–2060.

Charrasse S, Schroeder M, Gauthier-Rouviere C, Ango F, Cassimeris L, Gard DL, Larroque C (1998). The TOGp protein is a new human microtubule-associated protein homologous to the Xenopus XMAP215. J Cell Sci 111, 1371–1383.

Cooper JR, Wagenbach M, Asbury CL, Wordeman L (2010). Catalysis of the microtubule on-rate is the major parameter regulating the depolymerase activity of MCAK. Nat Struct Mol Biol 17, 77–82.

Desai A, Verma S, Mitchison TJ, Walczak CE (1999). Kin I kinesins are microtubule-destabilizing enzymes. Cell 96, 69–78.

Domnitz SB, Wagenbach M, Decarreau J, Wordeman L (2012). MCAK activity at microtubule tips regulates spindle microtubule length to promote robust kinetochore attachment. J Cell Biol 197, 231–237.

Du Y, English CA, Ohi R (2010). The kinesin-8 Kif18A dampens microtubule plus-end dynamics. Curr Biol 20, 374–380.

Ertych N, Stolz A, Stenzinger A, Weichert W, Kaulfuss S, Burfeind P, Aigner A, Wordeman L, Bastians H (2014). Increased microtubule assembly rates influence chromosomal instability in colorectal cancer cells. Nat Cell Biol 16, 779–791.

Gardner MK, Zanic M, Gell C, Bormuth V, Howard J (2011). Depolymerizing kinesins Kip3 and MCAK shape cellular microtubule architecture by differential control of catastrophe. Cell 147, 1092–1103.

Gay DA, Sisodia SS, Cleveland DW (1989). Autoregulatory control of beta-tubulin mRNA stability is linked to translation elongation. Proc Natl Acad Sci USA 86, 5763–5767.

Gay DA, Yen TJ, Lau JT, Cleveland DW (1987). Sequences that confer beta-tubulin autoregulation through modulated mRNA stability reside within exon 1 of a beta-tubulin mRNA. Cell 50, 671–679.

Gonzalez-Garay ML, Cabral F (1996). alpha-Tubulin limits its own synthesis: evidence for a mechanism involving translational repression. J Cell Biol 135, 1525–1534.

Grimaldi AD, Fomicheva M, Kaverina I (2013). Ice recovery assay for detection of Golgi-derived microtubules. Methods Cell Biol 118, 401–415.

Gupta ML Jr, Carvalho P, Roof DM, Pellman D (2006). Plus end-specific depolymerase activity of Kip3, a kinesin-8 protein, explains its role in positioning the yeast mitotic spindle. Nat Cell Biol 8, 913–923.

Hafner J, Mayr MI, Mockel MM, Mayer TU (2014). Pre-anaphase chromosome oscillations are regulated by the antagonistic activities of Cdk1 and PP1 on Kif18A. Nat Commun 5, 4397.

Helenius J, Brouhard G, Kalaidzidis Y, Diez S, Howard J (2006). The depolymerizing kinesin MCAK uses lattice diffusion to rapidly target microtubule ends. Nature 441, 115–119.

Honnappa S, Gouveia SM, Weisbrich A, Damberger FF, Bhavesh NS, Jawhari H, Grigoriev I, van Rijssel FJ, Buey RM (2009). An EB1-binding motif acts as a microtubule tip localization signal. Cell 138, 366–376.

Hu CK, Coughlin M, Field CM, Mitchison TJ (2011). KIF4 regulates midzone length during cytokinesis. Curr Biol 21, 815–824.

Hunter AW, Caplow M, Coy DL, Hancock WO, Diez S, Wordeman L, Howard J (2003). The kinesin-related protein MCAK is a microtubule depolymerase that forms an ATP-hydrolyzing complex at microtubule ends. Mol Cell 11, 445–457.

Inoue T, Heo WD, Grimley JS, Wandless TJ, Meyer T (2005). An inducible translocation strategy to rapidly activate and inhibit small GTPase signaling pathways. Nat Methods 2, 415–418.

Masuda N, Shimodaira T, Shiu SJ, Tokai-Nishizumi N, Yamamoto T, Ohsugi M (2011). Microtubule stabilization triggers the plus-end accumulation of Kif18A/kinesin-8. Cell Struct Funct 36, 261–267.

Montenegro Gouveia S, Leslie K, Kapitein LC, Buey RM, Grigoriev I, Wagenbach M, Smal I, Meijering E, Hoogenraad CC, Wordeman L, *et al.* (2010). In vitro reconstitution of the functional interplay between MCAK and EB3 at microtubule plus ends. Curr Biol 20, 1717–1722.

Moore AT, Rankin KE, von Dassow G, Peris L, Wagenbach M, Ovechkina Y, Andrieux A, Job D, Wordeman L (2005). MCAK associates with the tips of polymerizing microtubules. J Cell Biol 169, 391–397.

Nunes Bastos R, Gandhi SR, Baron RD, Gruneberg U, Nigg EA, Barr FA (2013). Aurora B suppresses microtubule dynamics and limits central spindle size by locally activating KIF4A. J Cell Biol 202, 605–621.

Odell GM, Foe VE (2008). An agent-based model contrasts opposite effects of dynamic and stable microtubules on cleavage furrow positioning. J Cell Biol 183, 471–483.

Ovechkina Y, Wagenbach M, Wordeman L (2002). K-loop insertion restores microtubule depolymerizing activity of a "neckless" MCAK mutant. J Cell Biol 159, 557–562.

Pachter JS, Yen TJ, Cleveland DW (1987). Autoregulation of tubulin expression is achieved through specific degradation of polysomal tubulin mRNAs. Cell 51, 283–292.

Rizk RS, Bohannon KP, Wetzel LA, Powers J, Shaw SL, Walczak CE (2009). MCAK and paclitaxel have differential effects on spindle microtubule organization and dynamics. Mol Biol Cell 20, 1639–1651.

Rizk RS, Discipio KA, Proudfoot KG, Gupta ML Jr (2014). The kinesin-8 Kip3 scales anaphase spindle length by suppression of midzone microtubule polymerization. J Cell Biol 204, 965–975.

Schindelin J, Arganda-Carreras I, Frise E, Kaynig V, Longair M, Pietzsch T, Preibisch S, Rueden C, Saalfeld S, Schmid B, *et al.* (2012). Fiji: an open-source platform for biological-image analysis. Nat Methods 9, 676–682.

Srayko M, Kaya A, Stamford J, Hyman AA (2005). Identification and characterization of factors required for microtubule growth and nucleation in the early C. elegans embryo. Dev Cell 9, 223–236.

Stepanova T, Slemmer J, Hoogenraad CC, Lansbergen G, Dortland B, De Zeeuw CI, Grosveld F, van Cappellen G, Akhmanova A, Galjart N (2003). Visualization of microtubule growth in cultured neurons via the use of EB3-GFP (end-binding protein 3-green fluorescent protein). J Neurosci 23, 2655–2664.

Stolz A, Ertych N, Bastians H (2015). A phenotypic screen identifies microtubule plus end assembly regulators that can function in mitotic spindle orientation. Cell Cycle 14, 827–837.

Stumpff J, Du Y, English CA, Maliga Z, Wagenbach M, Asbury CL, Wordeman L, Ohi R (2011). A tethering mechanism controls the processivity and kinetochore-microtubule plus-end enrichment of the kinesin-8 Kif18A. Mol Cel 43, 764–775.

Stumpff J, von Dassow G, Wagenbach M, Asbury C, Wordeman L (2008). The kinesin-8 motor Kif18A suppresses kinetochore movements to control mitotic chromosome alignment. Dev Cell 14, 252–262.

Stumpff J, Wagenbach M, Franck A, Asbury CL, Wordeman L (2012). Kif18A and chromokinesins confine centromere movements via microtubule growth suppression and spatial control of kinetochore tension. Dev Cell 22, 1017–1029.

Su X, Arellano-Santoyo H, Portran D, Gaillard J, Vantard M, Thery M, Pellman D (2013). Microtubule-sliding activity of a kinesin-8 promotes spindle assembly and spindle-length control. Nat Cell Biol 15, 948–957.

Suh BC, Inoue T, Meyer T, Hille B (2006). Rapid chemically induced changes of PtdIns(4,5)P2 gate KCNQ ion channels. Science 314, 1454–1457.

Ufret-Vincenty CA, Klein RM, Hua L, Angueyra J, Gordon SE (2011). Localization of the PIP2 sensor of TRPV1 ion channels. J Biol Chem 286, 9688–9698.

Varga V, Helenius J, Tanaka K, Hyman AA, Tanaka TU, Howard J (2006). Yeast kinesin-8 depolymerizes microtubules in a length-dependent manner. Nat Cell Biol 8, 957–962.

Wagenbach M, Domnitz S, Wordeman L, Cooper J (2008). A kinesin-13 mutant catalytically depolymerizes microtubules in ADP. J Cell Biol 183, 617–623.

Walczak CE, Gayek S, Ohi R (2013). Microtubule-depolymerizing kinesins. Annu Rev Cell Dev Biol 29, 417–441.

Wandke C, Barisic M, Sigl R, Rauch V, Wolf F, Amaro AC, Tan CH, Pereira AJ, Kutay U, Maiato H, *et al.* (2012). Human chromokinesins promote chromosome congression and spindle microtubule dynamics during mitosis. J Cell Biol 198, 847–863.

Weaver LN, Ems-McClung SC, Stout JR, LeBlanc C, Shaw SL, Gardner MK, Walczak CE (2011). Kif18A uses a microtubule binding site in the tail for plus-end localization and spindle length regulation. Curr Biol 21, 1500–1506.

Wordeman L, Wagenbach M, von Dassow G (2007). MCAK facilitates chromosome movement by promoting kinetochore microtubule turnover. J Cell Biol 179, 869–879.

Yen TJ, Gay DA, Pachter JS, Cleveland DW (1988). Autoregulated changes in stability of polyribosome-bound beta-tubulin mRNAs are specified by the first 13 translated nucleotides. Mol Cell Biol 8, 1224–1235.

Zhai Y, Borisy GG (1994). Quantitative determination of the proportion of microtubule polymer present during the mitosis-interphase transition. J Cell Sci 107, 881–890.

Zhou J, Shu HB, Joshi HC (2002). Regulation of tubulin synthesis and cell cycle progression in mammalian cells by gamma-tubulin-mediated microtubule nucleation. J Cell Biochem 84, 472–483.